Carcinogenesis vol.34 no.3 pp.577–586, 2013
doi:10.1093/carcin/bgs381
Advance Access publication December 7, 2012

Epigenetic activation of the MiR-200 family contributes to H19-mediated metastasis suppression in hepatocellular carcinoma

Ling Zhang[1,†], Fu Yang[1,†], Ji-hang Yuan[1,†], Sheng-xian Yuan[2,†], Wei-ping Zhou[2], Xi-song Huo[1], Dan Xu[1], Hai-shan Bi[1], Fang Wang[1] and Shu-han Sun[1,*]

[1]Department of Medical Genetics, Second Military Medical University, Shanghai, China and [2]The Third Department of Hepatic Surgery, Eastern Hepatobiliary Hospital, Second Military Medical University, Shanghai, China

*To whom correspondence should be addressed. Tel: +86 021 81871054; Fax: +86 021 81871053;
Email: shsun@vip.sina.com
Correspondence may also be addressed to Fang Wang. Tel: +86 021 81871054; Fax: +86 021 81871053;
Email: wfsjz70@gmail.com

Although numerous long non-coding RNAs (lncRNAs) have been identified in mammals, many of their biological roles remain to be characterized. Early reports suggest that H19 contributes to carcinogenesis, including hepatocellular carcinoma (HCC). Examination of the Oncomine resource showed that most HCC cases express H19 at a level that is comparable with the liver, with a tendency toward lower expression. This is consistent with our previous microarray data and indicates a more complicated role of H19 in HCC that needs to be characterized. In this study, the expression level of H19 was assessed in different regions of HCC patients' liver samples. Loss- and gain-of-function studies on this lncRNA in the HCC cell lines, SMMC7721 and HCCLM3, were used to characterize its effects on gene expression and to assess its effect on HCC metastasis both *in vitro* and *in vivo*. In this study, we show that H19 was underexpressed in intratumoral HCC tissues (T), as compared with peritumoral tissues (L). Additionally, low T/L ratio of H19 predicted poor prognosis. H19 suppressed HCC progression metastasis and the expression of markers of epithelial-to-mesenchymal transition. Furthermore, H19 associated with the protein complex hnRNP U/PCAF/RNAPol II, activating miR-200 family by increasing histone acetylation. The results demonstrate that H19 can alter the miR-200 pathway, thus contributing to mesenchymal-to-epithelial transition and to the suppression of tumor metastasis. These data provide an explanation for the hitherto puzzling literature on the relationship between H19 and cancer, and could suggest the development of combination therapies that target H19 and the miR-200 family.

Introduction

Hepatocellular carcinoma (HCC) is one of the leading cause of cancer death in China (1,2). The extremely poor prognosis of patients with HCC is largely due to the high frequency of tumor recurrence or metastasis after surgical resection. However, the molecular mechanisms underlying recurrence or metastasis in HCC remain largely unknown. Epithelial-to-mesenchymal (EMT) and mesenchymal-to-epithelial transitions play crucial roles in the progress of cancer metastasis. In particular, EMT has been found to contribute to the metastatic dissemination of the tumor and the acquisition of therapeutic resistance (3,4). Recent data have also demonstrated that epigenetic changes, such as microRNAs, histone modifications and DNA methylation, are involved in cancer metastasis (5–8). Specifically, the miR-200 family has been found to inhibit epithelial–mesenchymal transition and cancer cell migration (9,10).

Recently, long non-coding RNAs (LncRNAs) encoded in human genome have been shown to serve as important regulatory transcripts and may have other previously unappreciated functions (11–13). For example, they can serve as scaffolds, aiding the association of proteins with genomic DNA (14–17). In our recent study, we identified non-overlapping signatures of a small number of lncRNAs that are aberrantly expressed in human Hepatitis B virus (HBV)-related HCC compared with matched peritumoral tissues (18). Among these lncRNAs, H19 was found to play a potential role in HCC progression (19). Past studies have shown a strong association between H19 and carcinogenesis in several types of cancers, including liver cancer (20–26). In HCC, the expression of H19 usually changes from monoallelic to biallelic through aberrant DNA methylation (24–26). However, the relationship between H19 and HCC prognosis and the underlying mechanisms by which H19 may contribute to HCC are still largely unknown.

Recent studies have shown that well-known oncogenes, such as c-myc (27) and the androgen receptor (28), can also act as suppressors of cell motility, invasiveness and metastasis. In this study, we found that H19 promotes HCC tumor growth, which is consistent with previous reports. However, H19 can also upregulate the miR-200 family, thus suppressing the rate of tumor metastasis in advanced stages of HCC. Our findings provide new insights as to how lncRNAs can regulate the expression of small non-coding RNAs.

Abbreviations: ChIP, chromatin immunoprecipitation; EMT, epithelial-to-mesenchymal transition; HCC, hepatocellular carcinoma; HDAC, histone deacetylase; L, peritumoral tissues; LncRNA, long non-coding RNA; mRNA, messenger RNA; N, remote relative normal tissue; qRT–PCR, quantitative reverse transcription-PCR; RIP, RNA immunoprecipitation; siRNA, small interfering RNA; T, central of the tumor.

[†]These authors contributed equally to this work.

Materials and methods

Patient samples

In this study, matched tumor samples and non-cancerous hepatic tissues were obtained from HCC patients, and normal samples were randomly obtained with informed consent from the Eastern Hospital of Hepatobiliary (Second Military Medical University, Shanghai, China). Studies using human tissues were reviewed and approved by the Committees for Ethical Review of Research involving Human Subjects of Second Military Medical University (Shanghai, China). The patient samples were from 113 patients. The period of follow up of all patients is 1–24 months, with a median of 21 months. Paired samples of the primary tumor (T, center of tumors) and adjacent non-tumor tissue (L, <2 cm apart from the tumor tissues) were compared. In 33 patients, remote normal tissue (N, greater than at least 3 cm far away from the tumors) was sampled. In 113 patients, 41 non-invasive (without vascular invasion and subfoci of tumor and with intact tumor capsules) and 31 invasive (with vascular invasion and without intact tumor capsules) HCC samples were classified.

Reverse transcription reaction and quantitative real-time PCR

Total RNAs were extracted using Trizol reagent (Invitrogen, Carlsbad, CA). The first-strand cDNA was generated using the Reverse Transcription System Kit (Invitrogen, Carlsbad, CA). The primer used for H19-specific RT is referred to as 'H19-specific RT' (Supplementary Table 1, available at *Carcinogenesis* Online). Real-time PCR was performed according to a standard protocol using a StepOne Plus system (Applied Biosystems, Foster City, CA). As endogenous controls in each sample, glyceraldehyde 3-phosphate dehydrogenase was used for Taqman probe assays and β-actin was used for routine method assays. The real-time PCR reactions were performed in triplicate, and no template controls were included. Changes in expression were determined by the $2^{-\Delta\Delta CT}$ method. The primer sequences are presented in Supplementary Table 1, available at *Carcinogenesis* Online.

Generation of a stable cell line

Recombinant lentiviruses containing shRNA-1977 (LV-1977) or control (LV-NC) and shRNA-miR-200a (LV-miR-200a) or miRNA control (LV-miR Con) were purchased from GeneChem (Shanghai, China). To generate the stable cell line, 4×10^5 cells were transfected with 2×10^6 transducing units of lentiviruses, and the supernatant was removed after 24 h and replaced with complete culture medium. Infection efficiency was confirmed by RT–PCR 72 h after infection and the cells were selected with 2 μg/ml puromycin for 2 weeks.

Northern blotting

Northern blotting was performed according to manufacturer's instruction (NorthernMax®, LI-COR). Biotin probes were labeled by the incorporation of biotin-16-UTP (Roche) by in vitro transcription. The primers for H19 RNA probe are listed in Supplementary Table 1, available at *Carcinogenesis* Online. About 20 μg total RNA and 1 μg H19-specific probe were used for RNA hybridization.

Quantum dot fluorescent in situ hybridization

Paraffin-embedded tissue blocks were retrospectively retrieved from HCC patients. Quantum dot fluorescent *in situ* hybridization was performed to detect the presence of H19. A digoxin-labeled oligonucleotide probe (Supplementary Table 1, available at *Carcinogenesis* Online) indirectly labeled with streptavidin-conjugated quantum dots was used as described previously (18). Digoxigenin-labeled DNA probes for fluorescent *in situ* hybridization were synthesized by ShineGene (Shanghai, China). The probes are not located in the miR-675 region.

Small interfering RNA

Specific small interfering RNAs (siRNAs) targeting H19, P300/CBP-associated factor (PCAF), hnRNP U and the control siRNA were synthesized by GenePharma (Shanghai, China) as described (18) and are listed in Supplementary Table 1, available at *Carcinogenesis* Online. The cells were transfected with ~100 nM siRNA using the Lipofectamine 2000 kit (Invitrogen, Carlsbad, CA), according to the manufacturer's instructions. The cells were harvested 48 or 72 h after transfection.

Western blot analysis

Total cell lysates were prepared in a 1× sodium dodecyl sulfate buffer. Equal amounts of protein were separated by sodium dodecyl sulfate–polyacrylamide gel electrophoresis and transferred onto nitrocellulose membranes. Antibody dilutions used were 1:1000 for E-cadherin (Abcam, Hong Kong, China), 1:100 for N-cadherin (Abcam, Hong Kong, China), 1:1000 for Snail1 (Cell Signaling Technology, CA), 1:5000 for hnRNP U (Sigma–Aldrich), 1:1000 for PCAF (Cell Signaling Technology, CA), 1:1000 for RNA PolII (Millipore) and 1:5000 for β-actin (Sigma–Aldrich). After incubation with specific antibodies, the blots were incubated with Rdye800-conjugated goat anti-rabbit IgG and IRdye700-conjugated goat anti-mouse IgG and detected using an Odyssey infrared scanner (Li-Cor; Lincoln, NE).

Immunofluorescence

Cells were cultured on cover slips overnight and fixed with 4% paraformaldehyde for 20 min at room temperature. Samples were incubated with 0.2% Triton X-100 for 10 min and blocked for 2 h with the blocking solution purchased from Beyotime. Cells were then probed overnight at 4ºC with a diluted primary antibody, followed by a secondary antibody for 2 h. The primary antibodies used were a mouse monoclonal antibody for E-cadherin (1:100, Abcam, Hong Kong, China), Twist1 (1:80, Abcam, Hong Kong, China) and a rabbit polyclonal antibody against N-cadherin (1:100 dilution; Abcam, Hong Kong, China). The secondary antibodies used were Alexa 488-conjugated anti-mouse IgG (Invitrogen, Carlsbad, CA) and Alexa 594-conjugated anti-rabbit IgG (Invitrogen, Carlsbad, CA). DNA was stained with 4′,6-diamidino-2-phenylindole. All images were collected using a fluorescence microscope (Carl Zeiss, Axio Imager).

RNA pulldown

RNA pulldown analysis was performed as described previously (18). Briefly, 1 mg of cell nucleic protein extracts was incubated with biotinylated H19 or antisense RNA. Streptavidin beads were used to pull down the associated proteins, which were washed briefly five times and boiled in sodium dodecyl sulfate buffer, and the retrieved protein was detected by the standard western blot technique.

RNA immunoprecipitation

We performed RNA immunoprecipitation (RIP) experiments using the Magna RIP™ RNA-Binding Protein Immunoprecipitation Kit (Millipore), according to the manufacturer's instructions. The hnRNP U antibody used for RIP was used at a dilution of 1:5000 (Sigma–Aldrich). The coprecipitated RNAs were detected by reverse transcription-PCR. Total RNAs (input controls) and isotype controls were assayed simultaneously to demonstrate that the detected signals were from RNAs that specifically bound to hnRNP U, PCAF and RNA PolII ($n = 3$ for each experiment). The gene-specific primers used for detecting H19 are presented in Supplementary Table 1, available at *Carcinogenesis* Online.

Transwell assay

The transwell assays (Corning Costar; Cambridge, MA) were performed as described previously (18). To assay the invasive capacity of tumor cells, the upper chamber of each transwell was coated with matrigel (BD Biosciences) that was wiped out after incubating for 48 h using a cotton swab. And the cells migrated to the lower chamber were then stained.

Wound closure assay

Cells were grown to confluency in 12-well chambers for 24 and 48 h. To ensure standardization, the wells were marked across the wounded area to ensure documentation of the same region. Cells were washed three times with phosphate-buffered saline and the wells were refilled with medium containing 1 mM hydroxy urea (Sigma–Aldrich) to inhibit cell division. Photos were taken at 0, 24 and 48 h using an Olympus IX70 inverted microscope. The area invaded by tumor cells was calculated using the Image J software.

Chromatin immunoprecipitation

We performed chromatin immunoprecipitation (ChIP) using the EZ ChIP™ Chromatin Immunoprecipitation Kit for cell line samples (Millipore, Bedford, MA) and the EpiQuik Tissue Acetyl-Histone H3 ChIP Kit for primary tissue samples (Epigentek Group Inc, NY). Briefly, we sonicated the crosslinked chromatin DNA into 200–1000 bp fragments. The chromatin was then immunoprecipitated using an anti-acetyl-histone H3 antibody and hnRNP U (1:5000) or PCAF (1:25). Normal mouse IgG was used as the negative control. Primer sequences are listed in Supplementary Table 1, available at *Carcinogenesis* Online.

Nude mouse HCC model

All animal experiments met the guidelines of the Second Military Medical University Animal Care Facility and the National Institutes of Health. An orthotopic liver tumor xenograft model was established in nude mice to assess the role of H19 suppression in tumors. HCCLM3 cells were infected with LV-1977 or LV-NC or both LV-1977 and LV-NC or LV-miR-200a at multiplicity of infection of 20, and stably expressing cells were selected. Next, ~5×10^6 cells in 0.1 ml phosphate buffered saline were injected subcutaneously into both flanks of the mouse. Once a subcutaneous tumor reached 1–1.5 cm in diameter, it was removed and cut into ~1–2 mm^3 cubes, which were implanted into the liver lobes of another group of nude mice. Mice were killed to observe the development of metastases 6 weeks after the treatments. All experiments were performed with at least six mice in each group, and all of the experiments were repeated three times. Weight kinetics of the mice was followed over a period of 6 weeks. Mean percent of body weight (±SEM) for each group was measured every 7 days. Data are from three independent experiments.

Statistical analysis

All the statistical analyses were performed using SPSS version 17.0 software. All P values were two sided, and differences were considered statistically significant for P values ≤ 0.05. The levels of H19 in HCC patients were compared by the Wilcoxon signed-rank test. The cumulative disease-free survival probability was evaluated using the Kaplan–Meier method, and differences were assessed using the log-rank test. For the other experiments, Fisher's exact tests, chi-squared tests and two-tailed Student's t-tests were performed as appropriate.

Results

Aberrant expression of H19 in human HCC tissues and low H19 RNA tumor/peritumoral ratio (T/L) predicts poor prognosis

We previously performed lncRNA microarray hybridization to compare the lncRNA gene expression profiles between HCC and paired peritumoral tissues (18). All four different probes representing H19 were downregulated in HCC compared with the adjacent non-cancerous hepatic tissues (Supplementary Table 2, available at *Carcinogenesis* Online). Next, we examined the expression of H19 in primary tumors from 33 HCC patients (T, intratumoral tumor tissues), their adjacent non-tumor tissues (L, <2 cm apart from the tumor tissues) and remote relative normal tissues (N, greater than at least 3 cm far away from the tumors). As the HOTS gene resides in H19 antisense strand (29), we performed gene-specific reverse transcription in order to only characterize the H19 transcript, and quantitative real-time PCR (qRT-PCR) was carried out using Taqman probes. Although H19 was dramatically upregulated in T in some cases, we found the expression of H19 was mostly elevated in L compared with T ($P = 0.008$) and N ($P = 0.001$) (Figure 1A). Next, H19 expression was analyzed in 80 more T and L samples, and we

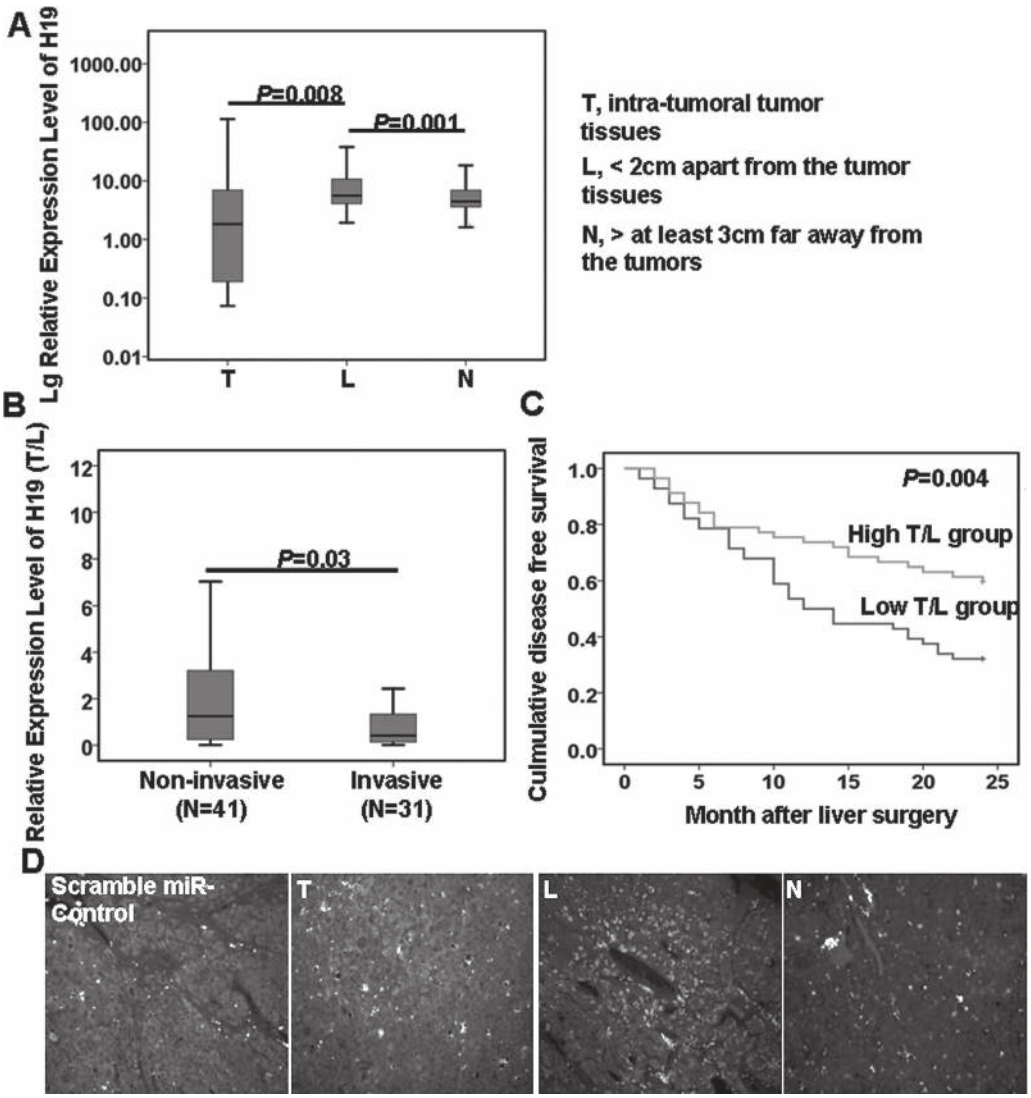

Fig. 1. Low T/L level of H19 expression predicts a poor prognosis in HCC and H19 RNA expression was most prominent at the boundary of the tumor nodule. (**A**) H19 expression in 33 paired samples of the primary tumor (T, intratumoral tissues), adjacent non-tumor tissue (L, <2 cm apart from the tumor tissues) and remote normal tissue (N, greater than at least 3 cm far away from the tumors) were analyzed by Taqman assay using the gene-specific reverse transcription primer and normalized to glyceraldehyde 3-phosphate dehydrogenase. Horizontal lines in the box plots represent the median, the boxes represent the interquartile range, and the whiskers represent the 2.5th and 97.5th percentiles. Significant differences were analyzed according to the Wilcoxon signed-rank test ($P < 0.05$). (**B**) The expression level of H19 was determined in 41 non-invasive (without vascular invasion and subfoci of tumor and with intact tumor capsules) and in 31 invasive (with vascular invasion and without intact tumor capsules) HCC samples from 113 patients. (**C**) H19 expression was measured in T and L tissues of HCC patients. Representative low-T/L expression (below the median value) and high-T/L expression (above the median value) were used in this analysis. The disease-free survival rates of 113 HCC patients, grouped according to whether they had low-T/L or high-T/L. The period of follow up of all patients is 1–24 months, with a median of 21 months after surgery. (**D**) H19 expression in hepatic and tumor tissues of the same patient, as demonstrated by digoxigenin-labeled *in situ* hybridization. The red signals, corresponding to probe hybridization, were located in both the nucleus and the cytoplasm. These signals were absent in the samples hybridized with a scramble miR-control probe. H19 expression was most prominent at the boundary of the tumor and was weak in the remote normal liver tissue and in the center of the tumor.

found that H19 expression was significantly lower in the invasive HCC samples than in the non-invasive HCC tumors (Figure 1B). This suggests that H19 may be involved in the aggressiveness of HCC.

Next, we investigated the relationship between the T/L ratio and the clinicopathological characteristics of these 113 patients. Correlation regression analysis indicated that low T/L ratio in tumor tissues was significantly correlated with intrahepatic tumor metastasis ($P = 0.02$) and tumor capsule integrity ($P = 0.02$) (Supplementary Table 3, available at *Carcinogenesis* Online). A Kaplan–Meier plot of disease-free survival of the 113 patients, who had been confirmed to have HCC, showed that low H19 T/L ratios were associated with shorter disease-free survival ($P = 0.004$) (Figure 1C). These results demonstrate that low levels of H19 in HCC tissues are correlated with a malignant cancer phenotype, particularly metastasis. Low H19 tumor/peritumoral ratio (T/L) also predicts poor prognosis. Clinicopathological prognostic factors were identified by Cox regression analysis and multivariable analysis showed that low H19 tumor/peritumoral ratio (T/L) was an independent predictor of poor outcome (Supplementary Table 4, available at *Carcinogenesis* Online).

To further characterize the level of H19 expression in HCC tissues, we used northern blotting and *in situ* hybridization to measure the levels of H19 RNA in the T, L and N. Northern blotting using the specific RNA probe showed that the full-length H19 RNA was expressed at higher levels in L (Supplementary Figure 1, available at *Carcinogenesis* Online), confirming the results we obtained by

qRT–PCR. *In situ* hybridization also showed that the H19 probe was most enriched in the areas surrounding HCC and was scattered in both nuclear and cytoplasmic areas compared with the scramble miR-control (Figure 1D). These results indicate that the expression of H19 is higher in the peritumoral area and low H19 tumor/peritumoral ratio (T/L) predicts poor prognosis.

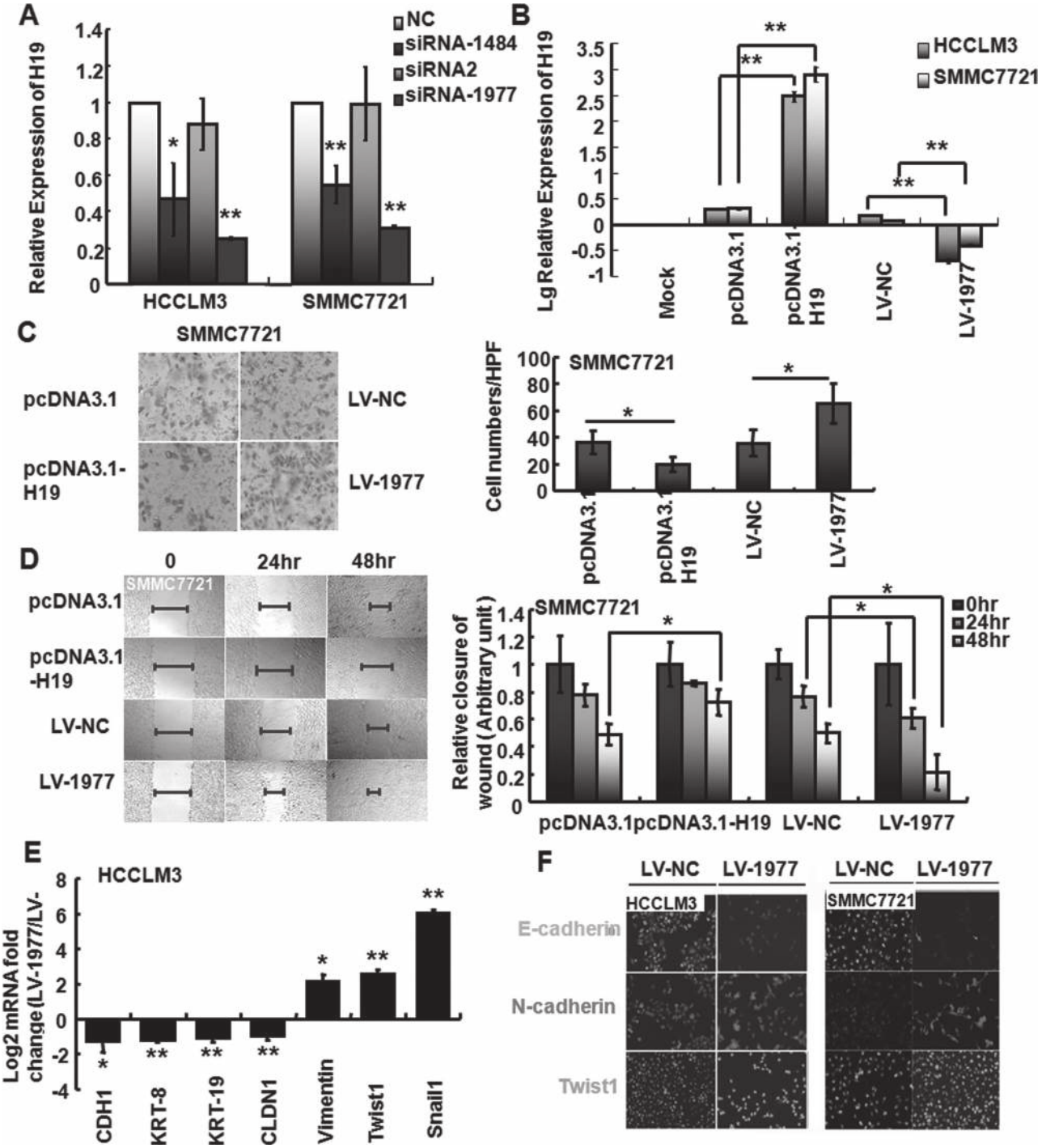

Fig. 2. H19 suppressed invasion and knockdown of H19-induced EMT markers in HCC cells *in vitro*. (**A**) HCCLLM3 (left) and SMMC7721 (right) cells were transfected with the transfection agent alone (Mock), with three different siRNAs against H19 (siRNA-1484, siRNA2 and siRNA-1977) or scramble-control siRNA (negative control, NC) for 48 h. The most efficient siRNA sequence was selected for further use. (**B**) The HCC cell lines SMMC7721 and HCCLM3 were transfected with control (pcDNA3.1) or pcDNA3.1-H19 and infected with LV-NC or LV-1977. H19 expression was analyzed by qRT–PCR after transfection for 48 h. (**C**) Transwell assays were used to assay the involvement of H19 in invasion. PcDNA3.1-H19- or pcDNA3.1-transfected and LV-1977- or LV-NC-infected SMMC7721 cells were incubated for 24 h, and counted under the microscope. The images are representative of at least three independent experiments. Original magnification ×100. The counted cell numbers per high power field are shown below. (**D**) Scrape motility assays were monitored at 0, 24 and 48 h after transfection, as described in Materials and methods. The images are representative of at least three independent experiments. Original magnification ×50. (**E**) qRT–PCR was performed to assess the mRNA levels of the epithelial markers E-cadherin, cytokeratin-8, cytokeratin-19 and claudin 1, the mesenchymal markers Vimentin and Snail1 and the EMT regulator Twist1 in LV-1977-infected versus LV-NC-infected HCCLM3 cells. The results, normalized against β-actin, are presented as log2, means ± SEM from three independent experiments. *$P < 0.05$, **$P < 0.01$. (**F**) Immunofluorescence assay showing labeled E-cadherin, N-cadherin and Twist1 in LV-NC-, LV-1977-infected HCCLM3 and SMMC7721 cells.

H19 suppresses the invasion of HCC cells in vitro

To investigate the biological effects of H19 loss-of-function in human HCC, the full-length cDNA sequence of H19 was cloned into the pcDNA3.1 (+) expression vector and siRNAs were used to knockdown H19. The efficiency of the three siRNA candidates was confirmed by qRT–PCR (Figure 2A). Next, we used the most efficient sequence, siRNA-1977, to generate cell lines stably expressing the shRNA. The HCCLM3 and SMMC7721 HCC cell lines were transfected with pcDNA3.1-H19 or pcDNA3.1 empty vector and infected with H19 shRNA-1977 lentiviral (LV-1977) or a control lentiviral (LV-NC) expression vector. Gene expression was confirmed by qRT–PCR (Figure 2B). Next, we investigated the effects of H19 expression on HCC cell growth and invasion *in vitro*. As shown in Supplementary Figure 2, available at *Carcinogenesis* Online, LV-1977 decreased the growth of SMMC7721 cells, as previously reported. However, the overexpression of H19 inhibited the invasion capacity of SMMC7721 cells and H19 knockdown promoted cell invasion *in vitro* (Figure 2C and D). These data support the hypothesis that H19 suppresses HCC metastasis. It has previously been reported that the H19-derived miR-675 can regulate tumor genes (21). We show that the ectopic overexpression of H19 could upregulate miR-675 RNA levels (Supplementary Figure 3A, available at *Carcinogenesis* Online), but that more miR-675 generated by H19 did not affect the metastatic ability of HCC cells (Supplementary Figure 3B, available at *Carcinogenesis* Online). Additionally, knockdown of miR-675 did not abolish the expression of the miR-200 family, which was induced by H19 (Supplementary Figure 3C, available at *Carcinogenesis* Online).

H19 inhibits invasion of HCC cells by reversing EMT

Next, to investigate how H19 inhibited invasion of HCC, and we reanalyzed previously generated microarray profiling data (http://www.ncbi.nlm.nih.gov/geo/query/acc.cgi?acc SE27462) (18). We found a correlation between the expression of H19 and EMT regulators (Supplementary Table 5, available at *Carcinogenesis* Online). As EMT is a critical event that contributes to tumor metastasis after tumor development (3,4), we investigated the effect of H19 on EMT. We analyzed the expression levels of previously reported molecular markers of EMT following H19 knockdown (30). The expression of epithelial markers, including E-cadherin (CDH1), cytokeratin-8 (KRT-8), cytokeratin-19 (KRT-19) and claudin 1 (CLDN1), were lower in cells in which H19 had been knocked down as compared with control cells. In contrast, the mesenchymal markers, including N-cadherin, Snail1, Vimentin and Twist1, were increased in HCCLM3 cells in which H19 had been knocked down (Figure 2E and F). This suggests that H19 may reverse the EMT response.

H19 upregulates the miR-200 family by associating with the HnRNP U/PCAF/RNA PolII complex and promoting histone acetylation

Given that H19 might be involved in EMT process and that miR-200 family plays a pivotal role in inhibiting EMT through regulation of target genes, including ZEB1 and ZEB2 (ZEB1/2) (9,10), we measured the relationship between H19 and other important regulators of EMT in HCC, including miR-200b. MiR-200b is a member of the miR-200 family and has been shown to be involved in HCC tumor pathogenesis (7). Analysis of a total of 40 tumor and peritumoral patient specimens revealed a correlation between

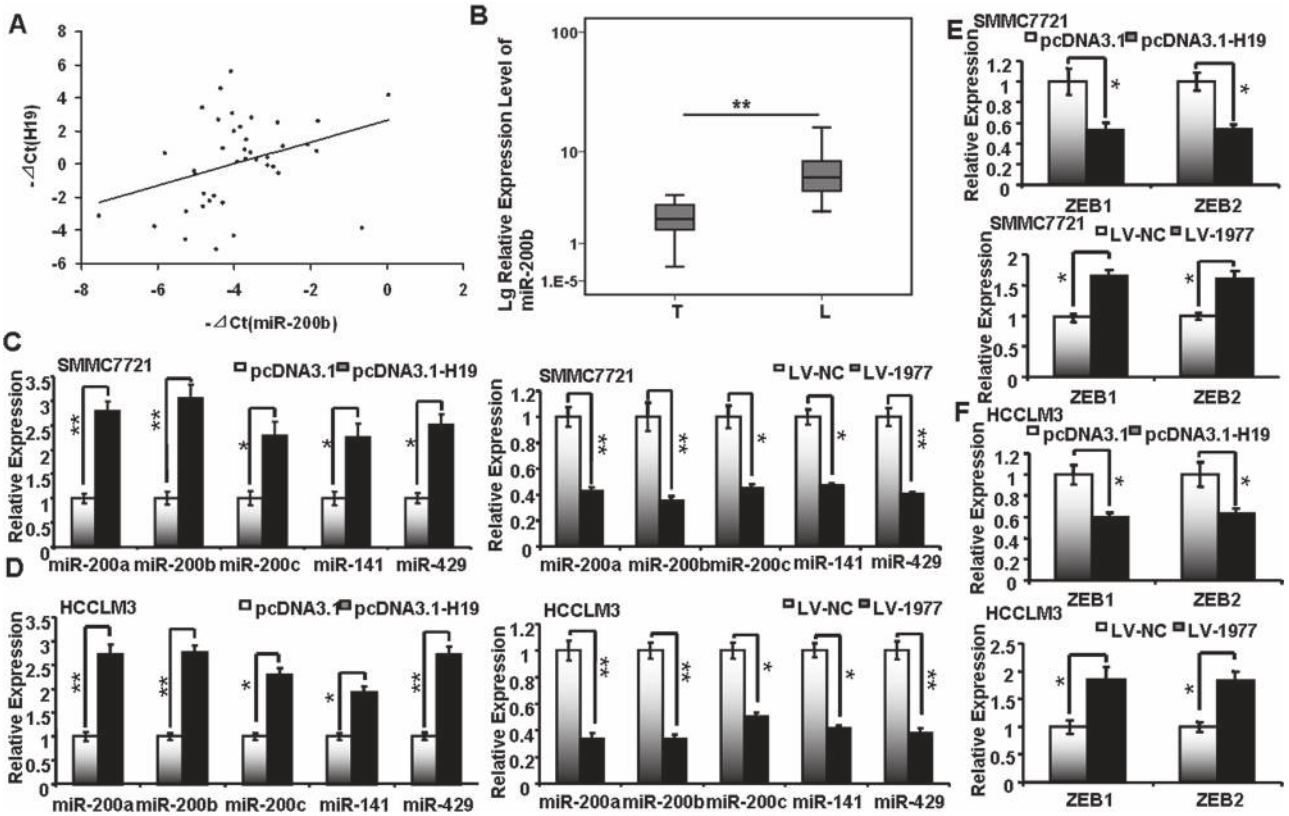

Fig. 3. Correlation between the expression of H19 and the miR-200 family. (**A**) Correlation analysis between the expression of H19 and miR-200b was examined in 40 paired tumor and peritumoral liver tissues derived from 20 patients. $r = 0.4$, $P = 0.03$. (**B**) The expression level of miR-200b in 20 paired tumor and peritumoral liver tissues (**$P < 0.01$). (**C** and **D**) Cells were transfected with pcDNA3.1 or pcDNA3.1-H19 and infected with LV-NC and LV-1977. Then, the expression levels of the miR-200 family members, miR-200a, miR-200b, miR-200c, miR-141 and miR-429, and their target, ZEB1/2, were measured using RT–PCR. *$P < 0.05$, **$P < 0.01$.

H19 expression and miR-200b levels ($r = 0.4$, $p = 0.03$) (Figure 3A and B). Thus, we asked whether H19 regulates miR-200 family in HCC cells, resulting in reversed EMT. The ectopic expression of the H19 upregulated miR-200 family, comprising miR-200a, miR-200b, miR-200c, miR-141 and miR-429, resulted in the down-regulation of their target genes, ZEB1/2. Conversely, knockdown of H19 suppressed the miR-200 family and upregulated ZEB1/2 (Figure 3C–F).

Recently, lncRNAs have been shown to be involved in molecular regulation pathways through their interaction with proteins (14–17). By RNA pull down assay (18) and western blot analysis, we verified that the full length of H19 can bind to the RNA-binding protein hnRNP U (Figure 4A). hnRNP U has been reported to be a member of protein complex, hnRNP U/PCAF/RNA PolII (31). PCAF is a well-known histone acetylase (32), and we have shown previously that aberrant histone acetylation occurs in the miR-200 family promoter region, resulting in aberrant miR-200 expression in HCC (6). As H19 can upregulate all members of miR-200 family and RIP also displayed the association between H19 and hnRNP U/PCAF/RNA PolII (Figure 4B), we knocked down hnRNP U or PCAF by siRNA and found that this abolished the upregulation of the miR-200 family driven by H19 (Figure 4C and D).

Next, we investigated the effect of the H19–hnRNP U/PCAF/RNA PolII protein complex on the levels of histone H3 acetylation at sites upstream of the miR-200 family. Ectopic expression of H19 in two human HCC cell lines caused a significant enrichment of hnRNP U, PCAF and histone H3 acetylation in regions upstream of miR-200b-200a-429 and miR-200c-141 as compared with the negative control.

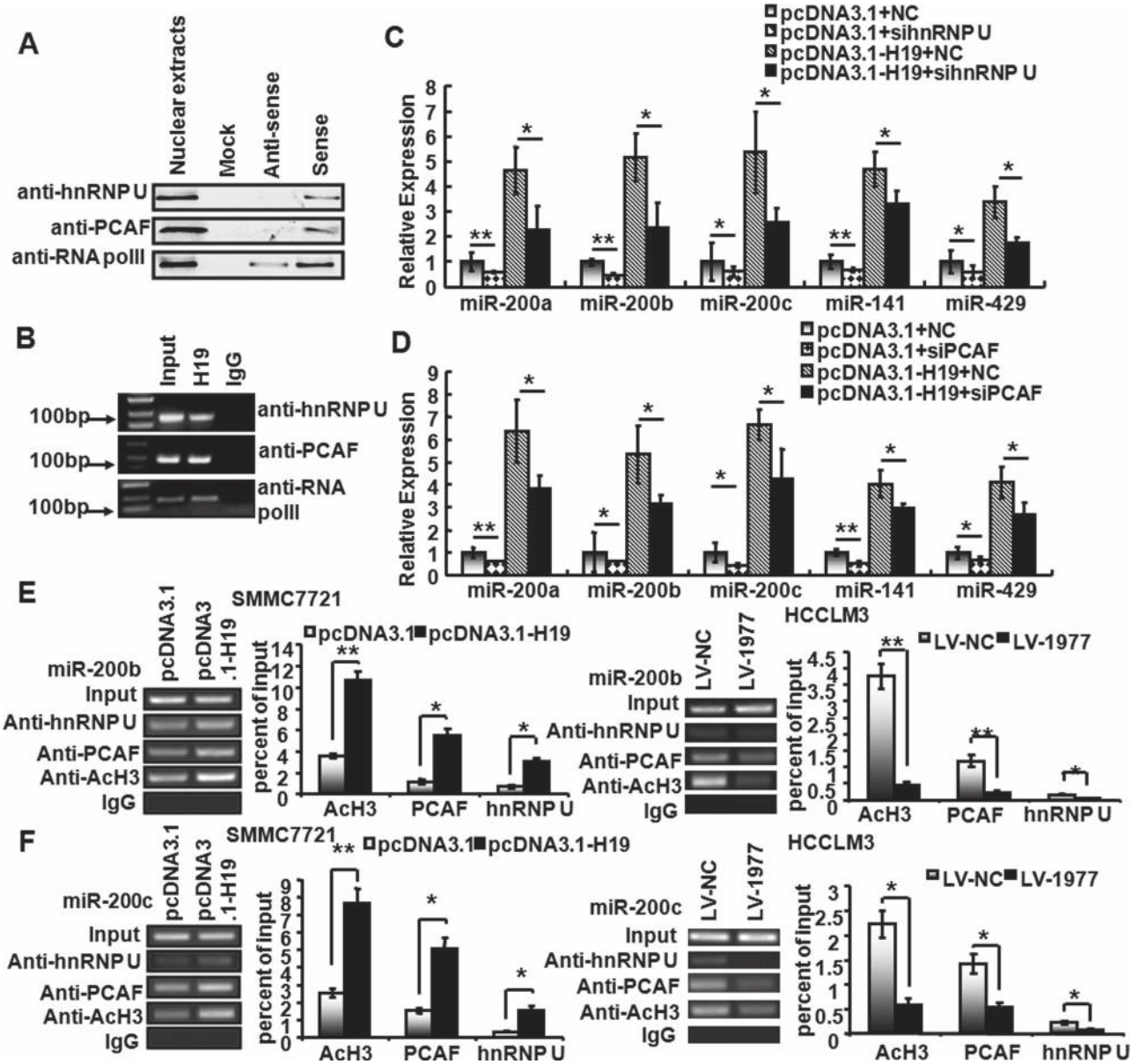

Fig. 4. The association of H19 with the hnRNP U/PCAF/POLII protein complex is critical for its regulation of the miR-200 family. (**A**) Western blot was performed after RNA pull down to show that H19 can bind to hnRNP U, PCAF and RNA PolII proteins *in vitro*. (**B**) RIP experiments were performed using the indicated antibodies for immunoprecipitation. Specific primers for H19 were used to detect H19. (**C** and **D**) Knockdown of PCAF or hnRNP U by siRNA reduced the upregulation of miR-200s induced by H19 in SMMC7721 cells. The asterisk indicates a significant change (*$P < 0.05$, **$P < 0.01$). (**E** and **F**) ChIP analyses in pcDNA3.1-H19- or pcDNA3.1-transfected SMMC7721 cells and LV-1977- or LV-NC-infected HCCLM3 cells were conducted on the miR-200c and miR-200b promoter regions using anti-acetyl-histone H3 (AcH3), PCAF and hnRNP U antibodies. Enrichment was determined relative to input controls. *$P < 0.05$, **$P < 0.01$. The data are the mean ± SD of three independent biological replicates.

Conversely, knockdown of H19 led to reduced hnRNP U and PCAF binding, and histone H3 acetylation (Figure 4E and F). In conclusion, these results indicate that H19 may associate with the hnRNP U/PCAF/RNA PolII complex to activate miR-200 family by histone acetylation.

Downregulation of H19 enhanced intrahepatic metastasis of HCC via miR-200 family pathway in vitro and in vivo

To investigated the role of the miR-200 family in H19-induced mesenchymal-to-epithelial and metastasis suppression, we ectopically overexpressed H19. This resulted in the upregulation of E-cadherin

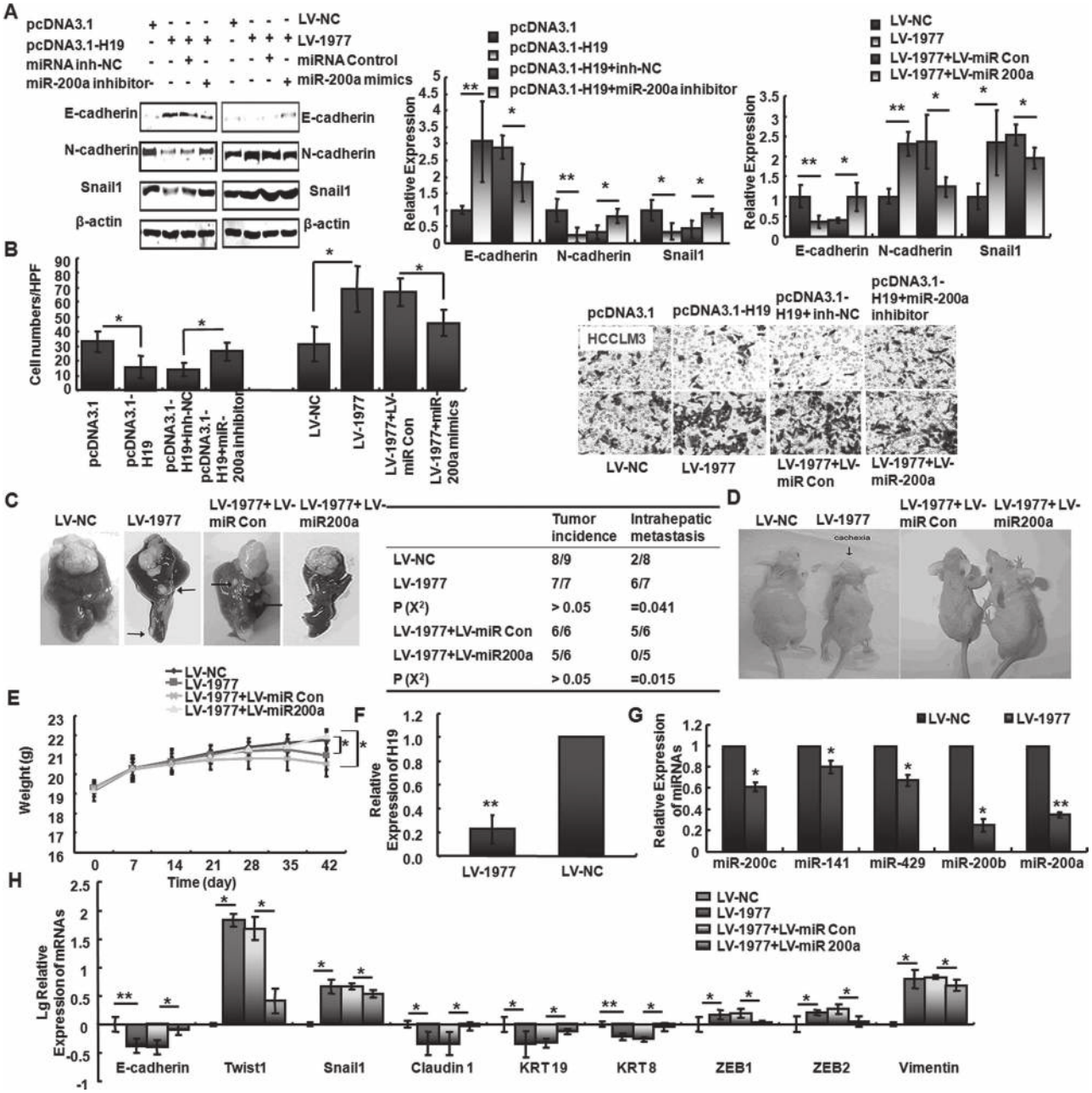

Fig. 5. H19 reverses EMT to suppress invasion by activating the miR-200 family in HCC. (**A**) Expression of indicated EMT molecules involved in EMT were detected by western blot, normalized toβ-actin. HCCLM3 cells were transfected with pcDNA3.1 or pcDNA3.1-H19 or pcDNA3.1-H19 cotransfected with miRNA inhibitor NC (inh-NC) or miR-200a inhibitor and infected with LV-NC or LV-1977 or LV-1977 coinfected with miRNA control (LV-miRNA Con) or LV-miR-200a. $*P < 0.05$, $**P < 0.01$. (**B**) Determination of miR-200a involvement in the regulation of cell invasion by H19 using transwell assays. HCCLM3 cells were treated as described above and incubated for 48 h. The images are representative of at least three independent experiments. (**C**) Left, metastatic nodes is indicated by arrowheads in the livers of LV-1977 group and the LV-1977 coinfected by LV-miR-Con group. Right, incidence of local and intrahepatic metastasis in orthotopic xenograft animal models. (**D**) Representative images of a mouse in each group 6 weeks after the orthotopic xenograft transplantation. And the LV-1977 group showed a obvious weight loss. (**E**) Body weight kinetics of 4-week-old male nude mice after intrahepatic transplantation followed over a period of 6 weeks. The mean body weight (±SEM) for each group is shown in weekly intervals. Data are from three independent experiments. $*P < 0.05$. (**F**) Six weeks after orthotopic xenograft transplantation, tumor tissues were removed and the knockdown efficiency was verified. $**P < 0.01$. (**G**) The expression levels of the miR-200 family members were measured in tumor tissues of LV-1977 and LV-NC groups. (**H**) The mRNA levels of the ZEB1, ZEB2 and other EMT regulatory molecules were assessed in the tumor tissues of the four groups. The results are shown as $\log_{10}$, normalized to β-actin and are presented as the means ± SEM from three independent experiments. $*P < 0.05$, $**P < 0.01$.

and the downregulation of N-cadherin, Snail1 protein levels in HCCLM3 and SMMC7721 cell lines (Figure 5A and Supplementary Figure 4, available at *Carcinogenesis* Online) and reduced invasion (Figure 5B). In contrast, knockdown of miR-200a in HCCLM3 cells ectopically overexpressing H19 led to decreased E-cadherin expression and increased N-cadherin and Snail1 expression (Figure 5A) and was associated with increased invasion ability compared with cells overexpressing H19 (Figure 5B). Conversely, by overexpressing miR-200a in H19 knockdown cells, EMT was reversed (Figure 5A and Supplementary Figure 4, available at *Carcinogenesis* Online) and less invasion ability were observed compared with HCCLM3 cells in which H19 had been knocked down (Figure 5B).

To test the possibility that H19 is involved in HCC metastasis *in vivo*, the HCCLM3 cells infected with LV-1977 or LV-NC and both LV-1977 and lentiviral-delivering miR-200a (LV-1977 + LV-miR-200a) or both LV-1977 and lentiviral-delivering miRNA control (LV-1977 + LV-miR Con) were subcutaneously implanted into the flanks of nude mice. Later, the implants were used for intrahepatic transplantation. Although the volume of the tumors in the group with low levels of H19 was smaller than that in the group with high levels of H19 (Supplementary Figure 5A and B, available at *Carcinogenesis* Online), and the group with low levels of H19 showed weaker Ki-67 and higher terminal deoxynucleotidyl transferase-mediated dUTP nick end labeling staining signals (Supplementary Figure 5C, available at *Carcinogenesis* Online). More important, *in vivo* experiment results indicated that the downregulation of H19 significantly facilitated tumor metastasis. This was shown by the observed increase in tumor intrahepatic metastasis. In the group overexpressing miR-200a, no metastasis loci were observed after knockdown of H19 (Figure 5C). Furthermore, the H19 knockdown group manifested significant cachexia (Figure 5D) and showed greater weight loss (Figure 5E). Six weeks later, the mice were killed and the tumor tissues were collected. H19 and miR-200 family RNA levels were measured using gene-specific RT–PCR. The expression of H19 remained significantly lower in the H19 knockdown group (Figure 5F). The reduced expression of H19 also induced changes in the expression of the miR-200 family (Figure 5G) and the EMT markers and ZEB1/2 in the xenografts (Figure 5H).

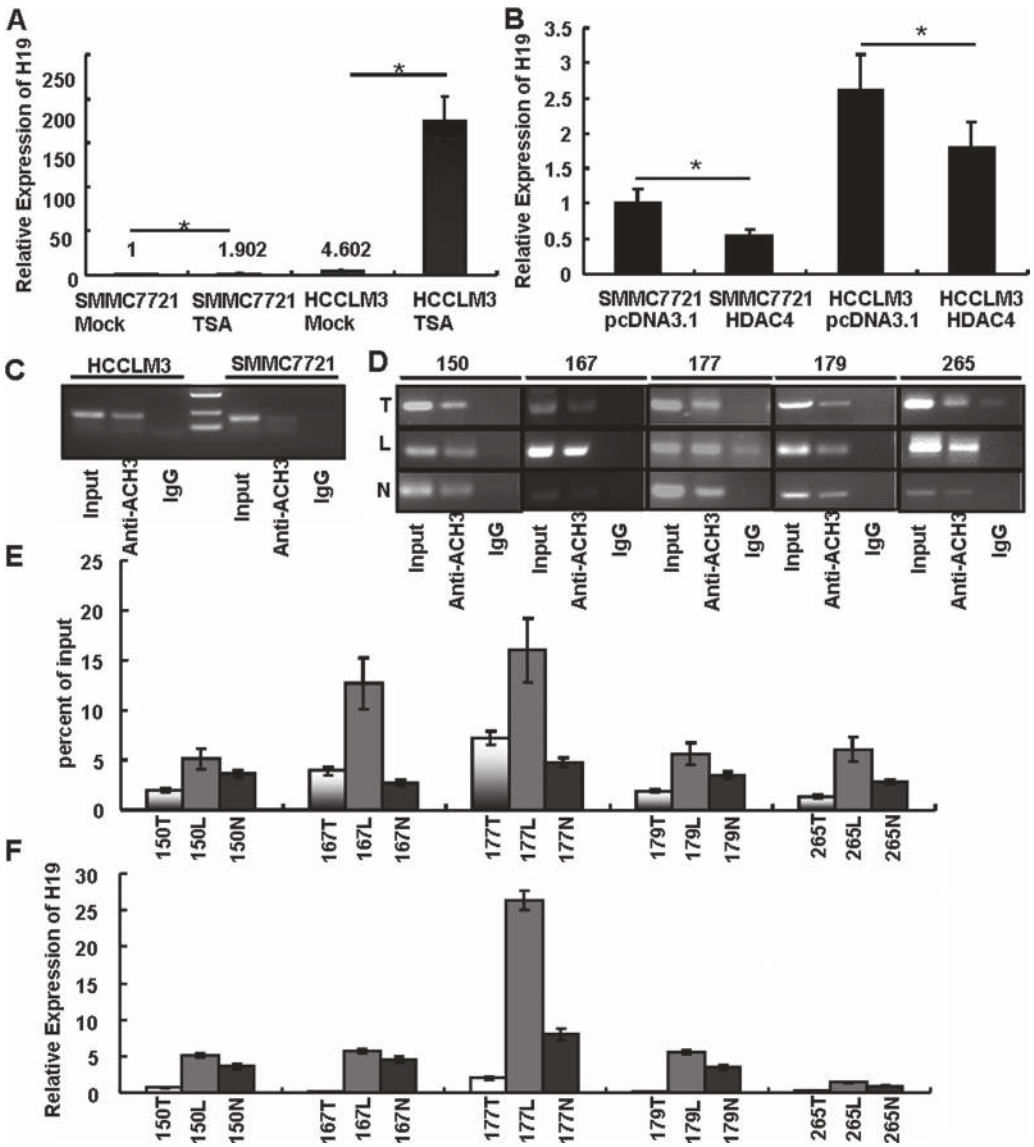

Fig. 6. Aberrant histone acetylation is responsible for the heterogeneous expression of H19 in different tissue regions. (**A**) Induction of H19 by treatment of HCCLM3 and SMMC7721 cells with 100 nM trichostatin A. *$P < 0.05$. (**B**) Downregulation of H19 by HDAC4 in cells. *$P < 0.05$. (**C**) ChIP analyses of cell lines conducted on the H19 promoter regions using an anti-AcH3. (**D** and **E**) ChIP analyses of hepatic tissues were performed on the H19 promoter region using anti-AcH3. Enrichment was determined relative to input controls. (**F**) The expression of H19 were detected by qRT–PCR in hepatic tissues that were analyzed in ChIP assay.

Together, these results reveal the functional significance of decreased H19 expression in HCC metastasis. Meanwhile, the miR-200 family that are involved in the reversion of EMT induced by H19, inhibited HCC metastasis.

Aberrant histone acetylation contributes to the differences in H19 expression patterns

To study the possible mechanisms underlying the non-uniform expression pattern of H19, we treated cells with the DNA methyltransferase inhibitor, 5-Aza-2′-deoxycytidine, and the histone deacetylase (HDAC) inhibitor, trichostatin A, as it has been previously reported that DNA methylation (25,26) and histone acetylation (33) can affect the expression of H19. Both inhibitors enhanced the expression of H19 (Figure 6A and Supplementary Figure 6A, available at *Carcinogenesis* Online). DNA methylation has been reported to be critical for the imprinting of the H19 gene and is associated with IGFII/H19 expression balance (25,26). Thus, we analyzed the patterns of the loss of imprinting and IGFII expression in paired HCC and paracarcinoma tissues. Although we found that loss of imprinting was not correlated with the expression level of H19 (Supplementary Figure 6B and C, available at *Carcinogenesis* Online), we often observed an imbalance in the expression levels of IGF2 and H19 (data not shown). Interestingly, H19 can be downregulated by the overexpression of the HDAC4 protein (Figure 6B). Next, we analyzed the patterns of histone acetylation enrichment in the promoter region of H19 in HCC cells and specimens by ChIP (Figure 6C–F). We found that the acetylation levels were higher in L than in either N or T tissues, which is in accordance with the expression pattern of H19. We suggest that aberrant histone acetylation might be responsible for the heterogeneity of H19 expression within tissues. However, the mechanism underlying the changes in histone modification patterns requires further investigation.

Discussion

These data indicate that the H19 RNA is involved in HCC aggressiveness. H19 was downregulated in invasive HCC specimens compared with non-invasive tissues. Additionally, a low H19 RNA T/L ratio was correlated with intrahepatic metastasis and with tumor capsule non-integrity in 113 patients. Accordingly, the Kaplan–Meier analysis indicated that, in general, patients with HCC who had low T/L ratios had worse prognosis than those with high ratios. Cox regression multivariable analysis showed that low H19 tumor/peritumoral ratio (T/L) was also an independent predictor of poor outcome. Our orthotopic xenograft experiments also indicated that tumors with reduced H19 expression generated more intrahepatic metastatic foci, suggesting that they had greater aggressive and metastatic properties. Therefore, the reduced expression profile of H19 correlated with disease deterioration, as demonstrated by our *in vitro* and *in vivo* studies.

In addition, we found that the reduced expression of H19 induced EMT by regulating the miR-200 family. Additionally, H19 associates with the protein complex hnRNPU/PCAF/RNAPolII, enhancing the histone acetylation in the upstream region of the miR-200 family. Thus, this provides new insights into the RNA regulation network, suggesting that lncRNA may not only target proteins but may also affect miRNA expression profiles through chromatin modification.

Notably, our results showed that the H19 RNA was enriched in the sections around the tumor tissues. This is in agreement with a previous report that H19 was most prominent at the boundary of the tumor nodule (26). We collected tissues from different sites of the patients' livers, and we defined the peritumoral tissues as the sections that were 2 cm away from the tumor tissues and the normal tissues as the sections that were at least 3 cm away from the tumors. This might explain why our results showed the downregulated H19 in tumors, compared with the peritumoral tissues, which is in contrast with previous reports (23).

Additionally, some genes do not present conventional expression patterns during tumor development and progression and the unique contributions of the surrounding non-cancerous tissues must be taken into account. For instance, hepatic androgen receptor was expressed at higher levels in peritumoral tissues than intratumoral tissues and may have dual and opposite roles in promoting HCC initiation, yet suppressing HCC metastasis (32). This suggests that the peritumoral tissues can influence cancer progression. The unconventional expression patterns of androgen receptor or H19 during cancer progression may be due to their functions in suppressing tumor progression after tumor initiation, but inhibiting tumor metastasis.

We also found that aberrant histone acetylation may be responsible for the heterogeneity of H19 expression in distinct locations of tissues. However, the mechanism underlying the changes in histone modification still needs to be further investigated. We have previously reported that miR-200a and HDAC4 form an autoregulatory loop in HCC (6). In this study, we show that the overexpression of HDAC4 can also suppress H19 expression, suggesting that H19 might also be involved in the autoregulation of miR-200a/HDAC.

Taken together, this study clearly demonstrates a crucial role for H19 in aggressive HCC. The prognostic significance of H19 and miR-200 family expression will help us to better predict the phenotype of the disease and the risk of recurrence. Individual therapy targeting the miR-200 family and H19 in combination may afford more curative effects.

Supplementary material

Supplementary Tables 1–5 and Figures 1–6 can be found at http://carcin.oxfordjournals.org/

Funding

National Natural Science Foundation of China (81071680, 81171936 and 81171937); Youth Start-up Funding of SMMU (2011QN02); Major Projects of National Science and Technology (2011ZXJ09103-07C); National Key Basic Research Program of China (2007CB512403, 2009CB522402).

Conflict of Interest Statement: None declared.

References

1. He,J. *et al.* (2005) Major causes of death among men and women in China. *N. Engl. J. Med.*, **353**, 1124–1134.
2. Parkin,D.M. *et al.* (2001) Estimating the world cancer burden: Globocan 2000. *Int. J. Cancer*, **94**, 153–156.
3. Marijon,H. *et al.* (2011) Epithelial-to-mesenchymal transition and acquired resistance to sunitinib in a patient with hepatocellular carcinoma. *J. Hepatol.*, **54**, 1073–1078.
4. Kim, J. *et al.* (2010) Epithelial-mesenchymal transition gene signature to predict clinical outcome of hepatocellular carcinoma. *Cancer Sci.*, **101,** 1521–1528.
5. Frau,M. *et al.* (2012) Role of transcriptional and post-transcriptional regulation of methionine adenosyltransferases in liver cancer progression. *Hepatology*, **56**, 165–175.
6. Yuan,J.H. *et al.* (2011) The histone deacetylase 4/SP1/microrna-200a regulatory network contributes to aberrant histone acetylation in hepatocellular carcinoma. *Hepatology*, **54**, 2025–2035.
7. Leung-Kuen Au,S. *et al.* (2012) Enhancer of zeste homolog 2 (EZH2) epigenetically silences multiple tumor suppressor miRNAs to promote liver cancer metastasis. *Hepatology*, **56,** 622–631.
8. Kong,K.L. *et al.* (2012) MicroRNA-375 inhibits tumour growth and metastasis in oesophageal squamous cell carcinoma through repressing insulin-like growth factor 1 receptor. *Gut*, **61**, 33–42.
9. Korpal,M. *et al.* (2008) The miR-200 family inhibits epithelial-mesenchymal transition and cancer cell migration by direct targeting of E-cadherin transcriptional repressors ZEB1 and ZEB2. *J. Biol. Chem.*, **283**, 14910–14914.
10. Hung,C.S. *et al.* (2012) MicroRNA-200a and -200b mediated hepatocellular carcinoma cell migration through the epithelial to mesenchymal transition markers. *Ann. Surg. Onco*, published online; doi:10.1245/s10434-012-2482-4.
11. Clark, M.B. *et al.* (2012) Genome-wide analysis of long noncoding RNA stability. *Genome Res.*, **22,** 885–898.
12. Liu,Y. *et al.* (2012) A genetic variant in long non-coding RNA HULC contributes to risk of HBV-related hepatocellular carcinoma in a Chinese population. *PLoS ONE*, **7**, e35145.

13. Ponting,C.P. *et al.* (2009) Evolution and functions of long noncoding RNAs. *Cell*, **136**, 629–641.
14. Tsai,M.C. *et al.* (2010) Long noncoding RNA as modular scaffold of histone modification complexes. *Science*, **329**, 689–693.
15. Guttman,M. *et al.* (2012) Modular regulatory principles of large non-coding RNAs. *Nature*, **482**, 339–346.
16. Ng,S.Y. *et al.* (2012) Human long non-coding RNAs promote pluripotency and neuronal differentiation by association with chromatin modifiers and transcription factors. *EMBO J.*, **31**, 522–533.
17. Guttman,M. *et al.* (2011) lincRNAs act in the circuitry controlling pluripotency and differentiation. *Nature*, **477**, 295–300.
18. Yang,F. *et al.* (2011) Long non-coding RNA high expressed in hepatocellular carcinoma (lncRNA-HEIH) facilitates tumor growth through enhancer of zeste homolog 2. *Hepatology*, **54,** 1679–1689.
19. Matouk,I.J. *et al.* (2007) The H19 non-coding RNA is essential for human tumor growth. *PLoS ONE*, **2**, e845.
20. Cui,H. *et al.* (1997) Inactivation of H19, an imprinted and putative tumor repressor gene, is a preneoplastic event during Wilms' tumorigenesis. *Cancer Res.*, **57**, 4469–4473.
21. Tsang,W.P. *et al.* (2010) Oncofetal H19-derived miR-675 regulates tumor suppressor RB in human colorectal cancer. *Carcinogenesis*, **31**, 350–358.
22. Yoshimizu,T. *et al.* (2008) The H19 locus acts *in vivo* as a tumor suppressor. *Proc. Natl. Acad. Sci. U.S.A.*, **105**, 12417–12422.
23. Ariel,I. *et al.* (1998) Imprinted H19 oncofetal RNA is a candidate tumour marker for hepatocellular carcinoma. *MP, Mol. Pathol.*, **51**, 21–25.
24. Kim,K.S. *et al.* (1997) Biallelic expression of the H19 and IGF2 genes in hepatocellular carcinoma. *Cancer Lett.*, **119**, 143–148.
25. Gao,Z.H. *et al.* (2002) Association of H19 promoter methylation with the expression of H19 and IGF-II genes in adrenocortical tumors. *J. Clin. Endocrinol. Metab.*, **87**, 1170–1176.
26. Wu,J. *et al.* (2008) Hypomethylated and hypermethylated profiles of H19DMR are associated with the aberrant imprinting of IGF2 and H19 in human hepatocellular carcinoma. *Genomics*, **91**, 443–450.
27. Liu,H. *et al.* (2012) MYC suppresses cancer metastasis by direct transcriptional silencing of alpha(v) and beta(3) integrin subunits. *Nat. Cell Biol.*, **14,** 567–574.
28. Ma,W.L. *et al.* (2012) Hepatic androgen receptor suppresses hepatocellular carcinoma metastasis through modulation of cell migration and anoikis. *Hepatology*, **56**, 176–185.
29. Onyango,P. *et al.* (2011) A nucleolar protein, H19 opposite tumor suppressor (HOTS), is a tumor growth inhibitor encoded by a human imprinted H19 antisense transcript. *Proc. Natl. Acad. Sci. U.S.A.*, **108**, 16759–16764.
30. Fu,J. *et al.* (2011) p28GANK overexpression accelerates hepatocellular carcinoma invasiveness and metastasis via phosphoinositol 3-kinase/AKT/hypoxia-inducible factor-1α pathways. *Hepatology*, **53**, 181–192.
31. Obrdlik,A. *et al.* (2008) The histone acetyltransferase PCAF associates with actin and hnRNP U for RNA polymerase II transcription. *Mol. Cell. Biol.*, **28**, 6342–6357.
32. Jin,Q. *et al.* (2011) Distinct roles of GCN5/PCAF-mediated H3K9ac and CBP/p300-mediated H3K18/27ac in nuclear receptor transactivation. *EMBO J.*, **30**, 249–262.
33. Barsyte-Lovejoy,D. *et al.* (2006) The c-Myc oncogene directly induces the H19 noncoding RNA by allele-specific binding to potentiate tumorigenesis. *Cancer Res.*, **66**, 5330–5337.

Received August 17, 2012; revised November 5, 2012; accepted November 22, 2012